AIAA 81-0381R

Improved Finite-Difference Scheme for Transonic Airfoil Flowfield Calculations

Lee-Tzong Chen*
McDonnell Douglas Corporation, St. Louis, Mo.

Second-order quasiconservative and nonconservative finite-difference schemes, which yield second-order-accurate solutions in supersonic regions, have been developed for transonic flowfield calculations about airfoils. The solution accuracy is further improved by applying a third-order isoparametric element which improves the finite-difference approximations for velocity components and body boundary conditions. It is found that the discrepancies between first- and second-order, quasi- and fully conservative solutions are generally small for cases containing a single shock. However, the discrepancy is significant for cases containing double shocks. Furthermore, the present second-order quasiconservative scheme has been shown to provide better solution resolution near shocks than the second-order fully conservative scheme, and thus needs fewer grid points on the airfoil surface for an adequate prediction of shock strength and location.

Introduction

METHODS for computation of steady, inviscid transonic flowfields have reached a stage of development where they are gaining acceptance in aerodynamic design. Because of the complex nature of transonic flowfields, a large number of grid points is generally required on airfoil or wing surfaces for adequate prediction of shock strength and location. Furthermore, many configurations considered in aerodynamic design cannot be adequately treated by existing computer programs, in part because computer storage limitations do not permit the use of a grid that can resolve flowfield gradients about complex geometries when conventional finite-difference schemes are used. For instance, Ballhaus and Bailey[1] indicated that in many engineering applications, the storage limitations of the NASA Ames Research Center CDC 7600 do not allow adequate resolution of the flowfield about a simple isolated wing, nor about a wing-fuselage or more complex configurations. Poor computational resolution always results in shock-wave pressure gradients smeared over a greater chordwise distance than actually occurs. Lynch[2] showed that this shock smearing substantially degrades the accuracy of existing, coupled, viscous-inviscid calculations and may cause significant underprediction of the boundary-layer displacement thickness near the trailing edge. Therefore advanced, higher-order methods with increased accuracy for a fixed number of grid points are needed to alleviate storage problems and improve resolution near high-gradient regions, such as near leading and trailing edges and near shock waves, in inviscid transonic flowfield calculations.

Attempts to increase the order of accuracy of conventional finite-difference schemes for transonic flow computation have not received great emphasis, partly because characteristics of the conventional five-point (elliptic) operator are well known and well documented. Improving the order of accuracy of a transonic potential flow calculation requires consideration of two independent problems. The first problem is related to improving the order of accuracy of the flow equation approximation in subsonic regions. The second problem is related to improving the order of accuracy of artificial viscosities and/or densities to be added to the flow equation approximation in supersonic regions in order to reflect the directional bias of the flow.

By introducing an isoparametric third-order element, Chen and Caughey[3] developed a third-order-accurate finite-difference scheme for solving a locally transformed, full-potential equation. The transformation matrix and potential function are exact for a general cubic function of the dependent variables, therefore the scheme is third-order accurate in subsonic flows in terms of global truncation error. Although when applying finite-difference schemes, it is customary to be concerned primarily with the discretization error at control points where the finite-difference equation is satisfied, the global truncation error is of greater importance in solving the discretized equations resulting from either finite-difference or finite-element formulations. Third-order finite-difference schemes are less widely used than the conventional second-order schemes; however, the former have often been used in solving flow equations where first-derivative terms are more crucial in the solution process, for example in convective diffusion problems.[4] To improve the order of accuracy of the flow equations in supersonic regions, Jameson[5] introduced a second-order-accurate, fully conservative, artificial viscosity term which improves the solution accuracy in supersonic regions for certain cases but fails to provide converged solutions for strong shock cases. Ives and Liutermoza[6] developed a second-order-accurate nonconservative scheme which also improves the solution accuracy in supersonic regions; however, since their scheme is nonconservative, the degree to which conservation of mass is satisfied at the shock is not known.

In the present method, a local coordinate transformation is applied to uncouple the flow equation solver from the grid-generation step. A finite-difference approximation of the full potential is obtained by applying a second-[7] or a third-order[3] element, and by adding new second-order artificial viscosities in supersonic regions. The difference equations are solved for transonic flowfields about airfoils by an extrapolated relaxation scheme. Both nonconservative and quasiconservative solutions are obtained. Tentative comparison and assessment of present solutions vs conventional solutions are made in the context of computing flow around an airfoil where results from methods of well-established accuracy and reliability are available.

Presented as Paper 81-0381 at the AIAA 19th Aerospace Sciences Meeting, St. Louis, Mo., Jan. 12-15, 1981; submitted March 11, 1981; revision received July 30, 1981.

*Research Scientist, McDonnell Douglas Research Laboratories. Member AIAA.

Third-Order Finite-Difference Approximations

Isoparametric elements are commonly used, especially in finite-element analysis, to locally transform a curvilinear coordinate system to a convenient computational coordinate system. The trend to treat more and more complex geometries in finite-difference schemes for transonic flow calculations makes the use of body-conforming coordinates desirable, and therefore the use of isoparametric elements to transform coordinate systems has become popular. For example, first-order isoparametric elements were adopted by Jameson and Caughey[8] and by Caughey and Jameson[9] in formulating finite-volume schemes. Second-order (Fig. 1) and third-order (Fig. 2) isoparametric elements were adopted by Chen and Caughey[3,7] in formulating finite-difference representations of the two- and three-dimensional, full-potential equations for inlet flow calculations. The second-order element was also used by Chen[10] to improve the implementation of boundary conditions in a wing-body computer program FLO-27, based upon the Jameson and Caughey method.[8] Other higher-order elements are also under study; for example, both second- and fourth-order elements were considered by Deconinck and Hirsch.[11] Considering a third-order element[3] (Fig. 2), the physical coordinates x and y of a point p in the element are related to the computational coordinates X and Y by

$$x=\psi^T x_i \tag{1}$$

and

$$y=\psi^T y_i \tag{2}$$

where ψ^T is the transpose of ψ, a column vector of the third-order-element shape function given by

$$\psi=\frac{1}{36}\begin{Bmatrix} X(X+1)(X+2) & Y & (Y+1)(Y+2) \\ -3X(X+1)(X+2) & (Y-1) & (Y+1)(Y+2) \\ 3X(X+1)(X+2) & Y & (Y-1)(Y+2) \\ -X(X+1)(X+2) & Y & (Y+1)(Y-1) \\ 3(X-1)(X+1)(X+2) & Y & (Y+1)(Y-1) \\ -3X(X-1)(X+2) & Y & (Y+1)(Y-1) \\ X(X+1)(X-1) & Y & (Y+1)(Y-1) \\ -3X(X+1)(X-1) & Y & (Y-1)(Y+2) \\ 3X(X+1)(X-1) & (Y-1) & (Y+1)(Y+2) \\ -X(X+1)(X-1) & Y & (Y+1)(Y+2) \\ 3X(X-1)(X+2) & Y & (Y+1)(Y+2) \\ -3(X-1)(X+1)(X+2) & Y & (Y+1)(Y+2) \\ 9(X-1)(X+1)(X+2) & (Y-1) & (Y+1)(Y+2) \\ -9(X-1)(X+1)(X+2) & Y & (Y-1)(Y+2) \\ 9X(X-1)(X+2) & Y & (Y-1)(Y+2) \\ -9X(X-1)(X+2) & (Y-1) & (Y+1)(Y+2) \end{Bmatrix}$$

$$-2\le X\le 1; \quad -2\le Y\le 1 \tag{3}$$

The transpose of the column vectors of x and y mesh coordinates are given as

$$x_i^T=[x_1,x_2,\ldots x_{16}] \tag{4}$$

and

$$y_i^T=[y_1,y_2,\ldots y_{16}] \tag{5}$$

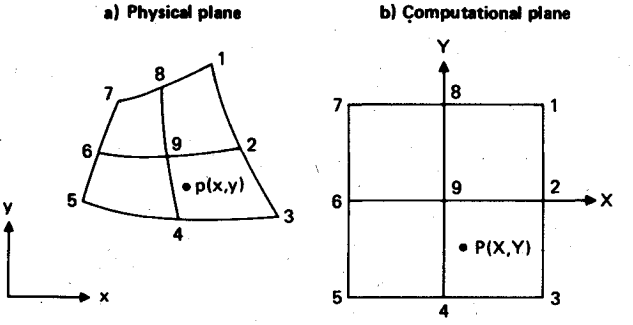

Fig. 1 Transformation of second-order element.

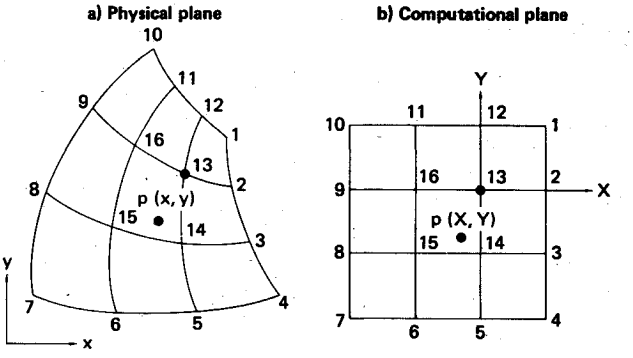

Fig. 2 Transformation of third-order element.

where (x_1,y_1), (x_2,y_2),... (x_{16},y_{16}) are coordinates of points 1, 2,... 16 in the physical plane, respectively (see Fig. 2).

The potential function ϕ at point p is given by

$$\phi=\psi^T\phi_i \tag{6}$$

where

$$\phi_i^T=[\phi_1,\phi_2,\ldots\phi_{16}] \tag{7}$$

and $\phi_1,\phi_2,\ldots\phi_{16}$ are values of ϕ at points 1, 2,... 16.

The equation for the velocity potential ϕ written in physical coordinates is

$$(a^2-u^2)\phi_{xx}+(a^2-v^2)\phi_{yy}-2uv\phi_{xy}=0 \tag{8}$$

where u and v are the velocity components in the x and y directions, respectively, and a is the local speed of sound determined from the energy equation

$$a^2=a_0^2-(\nu-1)(u^2+v^2)/2 \tag{9}$$

where a_0 is the stagnation speed of sound and ν the ratio of specific heats for the assumed, calorically perfect gas.

In the computational plane, Eq. (8) is rewritten as

$$C_1\phi_{XX}+C_2\phi_{YY}+C_3\phi_{XY}+C_4\phi_X+C_5\phi_Y=0 \tag{10}$$

where

$$C_1=[a^2(x_Y^2+y_Y^2)-(uy_Y-vx_Y)^2]/D^2 \tag{11}$$

$$C_2=[a^2(x_X^2+y_X^2)-(uy_X-vx_X)^2]/D^2 \tag{12}$$

$$C_3=-2[a^2(x_Xx_Y+y_Xy_Y) - (uy_Y-vx_Y)(uy_X-vx_X)]/D^2 \tag{13}$$

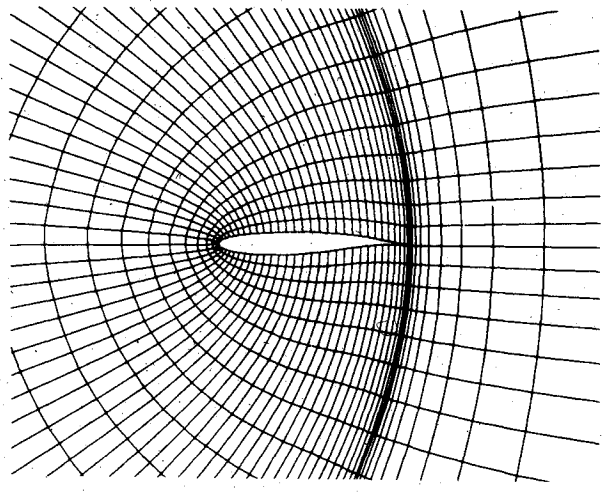

Fig. 3 Mapping-generated grid for a Korn airfoil.

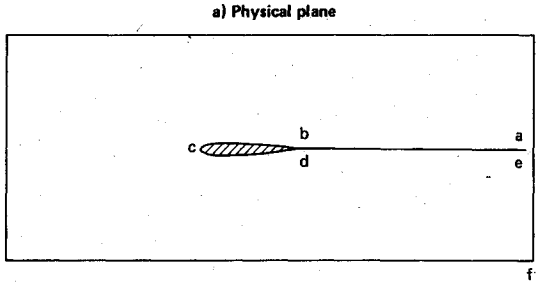

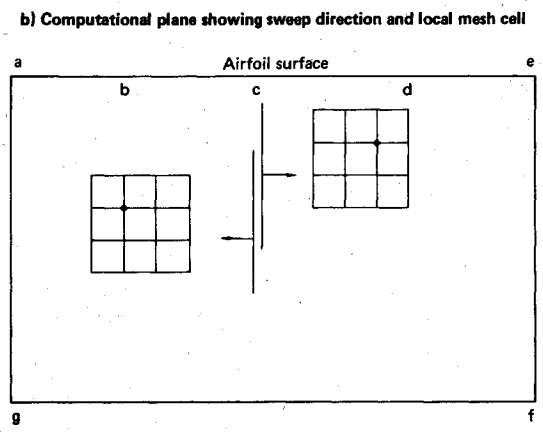

Fig. 4 Flowfield around an airfoil.

$$C_4=[(C_1y_{XX}+C_2y_{YY}+C_3y_{XY})x_Y - (C_1x_{XX}+C_2x_{YY}+C_3x_{XY})y_Y]/D \quad (14)$$

$$C_5=[(C_1x_{XX}+C_2x_{YY}+C_3x_{XY})y_X - (C_1y_{XX}+C_2y_{YY}+C_3y_{XY})x_X]/D \quad (15)$$

and

$$u=(y_Y\phi_X-y_X\phi_Y)/D \quad (16)$$

$$v=(x_X\phi_Y-x_Y\phi_X)/D \quad (17)$$

$$D=x_Xy_Y-x_Yy_X \quad (18)$$

The transformation coefficients x_X, y_X, x_Y, y_Y, x_{XX}, x_{YY}, x_{XY},... can be computed analytically, if an analytical coordinate transformation can be found, or numerically through finite-difference approximations. In order to uncouple the grid generation from the flow equation solver, it is convenient to compute the transformation coefficients numerically by differentiating Eqs. (1) and (2). The derivatives of the potential function, ϕ_X, ϕ_Y, ϕ_{XX}, ϕ_{YY}, and ϕ_{XY} are similarly computed using Eq. (6). Equation (10) is more compact than the transformed equation obtained in Ref. 7 and therefore can be treated more efficiently in computers. The equation is more general for formulating finite-difference approximations of the flow equation and boundary conditions than the one suggested in the finite-volume method by Jameson and Caughey.[8] To solve Eq. (10), the finite-difference approximation of Eq. (10) must be satisfied at every mesh point in the flowfield. It is convenient and always possible to arrange a local element in the computational plane so that the control point is located at $X=Y=0$ as shown in Fig. 4, where dots represent the control points. The transformation coefficients and derivatives of the potential function, derived using Eqs. (1), (2), and (6), are given in Ref. 3 and will not be repeated here. Since the highest degree of the shape functions used in Eq. (3) is the third degree, the finite-difference approximation to Eq. (10) thus obtained is third-order accurate.

Artificial Viscosities

In order to reflect the directional bias of supersonic flows, proper artificial viscosities or densities are generally added to the finite-difference approximation of the preceding sections in regions where the local Mach number exceeds unity. In conventional nonconservative schemes, upwind differences are used to approximate the second derivative of the potential function in the streamwise direction. In fully conservative schemes, artificial viscosity (or density) terms chosen to emulate the effect of this upwind differencing are added in divergence form. In the so-called quasiconservative schemes, the artificial viscosity is in divergence form but the flow equation is not. In Ref. 3, first-order-accurate nonconservative and quasiconservative schemes were introduced and will not be discussed here. In the following, second-order-accurate nonconservative and quasiconservative schemes will be introduced. For constructing the artificial viscosity, it is convenient to think of Eq. (8) as being rewritten in terms of a Cartesian system rotated into alignment with the local flow direction. If s and n are taken to be coordinates along and normal to the local velocity vector, then Eq. (8), after division by a^2, becomes

$$[1-(q^2/a^2)]\phi_{ss}+\phi_{nn}=0 \quad (19)$$

where q is the magnitude of the velocity. The second derivative of the potential function in the s direction can be expressed in terms of the computational variables as

$$\phi_{ss}=p_1\phi_{XX}+p_2\phi_{YY}+p_3\phi_{XY} \quad (20)$$

where

$$p_1=(uy_Y-vx_Y)^2/D^2 \quad (21)$$

$$p_2=(uy_X-vx_X)^2/D^2 \quad (22)$$

$$p_3=-2(uy_Y-vx_Y)(uy_X-vx_X)/D^2 \quad (23)$$

The first-derivative terms appearing in Eq. (19) are ignored for constructing the artificial viscosities since they generally play a secondary role in stabilizing the relaxation process.

In the second-order nonconservative scheme, upwind differences are used to approximate the contributions of ϕ_{XX} and ϕ_{YY} in the first term of Eq. (19). This use of upwind differences is equivalent to adding the following artificial

viscosity term H_{NC} to the finite-difference approximation of Eq. (10):

$$H_{NC}=\mu\{p_1(\Delta X)^2\phi_{XXXX}+p_2(\Delta Y)^2\phi_{YYYY}\} \tag{24}$$

where

$$\mu=\max[1-(q^2/a^2),0] \tag{25}$$

$$\phi_{XXXX}=4(\phi_{i,j}+\phi_{i-2m,j})-\phi_{i+m,j}-\phi_{i-3m,j}-6\phi_{i-m,j} \tag{26}$$

$$\phi_{YYYY}=4(\phi_{i,j}+\phi_{i,j-2n})-\phi_{i,j+n}-\phi_{i,j-3n}-6\phi_{i,j-n} \tag{27}$$

$$m=\begin{cases}1, & \text{if } U=y_Y u-x_Y v>0\\ -1, & \text{if } U<0\end{cases} \tag{28}$$

$$n=\begin{cases}1, & \text{if } V=x_X v-y_X u>0\\ -1, & \text{if } V<0\end{cases} \tag{29}$$

Although the nonconservative solutions do not ensure mass flux conservation across the shock, they usually are in good agreement with experimental data.[7]

In the second-order quasiconservative scheme, the following artificial viscosity H_{QC} is added to the finite-difference approximation of Eq. (10) in divergence form in supersonic regions:

$$\begin{aligned}H_{QC}&=(\Delta X)^2(\mu p_1\phi_{XX})_{XX}+(\Delta Y)^2(\mu p_2\phi_{YY})_{YY}\\&=(\mu p_1\phi_{XX})_{i-2m,j}-2(\mu p_1\phi_{XX})_{i-m,j}+(\mu p_1\phi_{XX})_{i,j}\\&+(\mu p_2\phi_{YY})_{i,j-2n}-2(\mu p_2\phi_{YY})_{i,j-n}+(\mu p_2\phi_{YY})_{i,j}\end{aligned} \tag{30}$$

In earlier work,[12] the addition of H_{QC} is continued at the first and second downstream subsonic points after the shock, such that the quantities $\mu p_1\phi_{XX}$ and $\mu p_2\phi_{YY}$ are conserved across the shock and implying that the mass flux is approximately conserved across the shock. However, at the first ($\mu_{i,j}=0$) and second ($\mu_{i,j}=\mu_{i-m,j}=\mu_{i,j-n}=0$) downstream subsonic points, H_{QC} becomes a zeroth-order term which will not diminish as the mesh size goes to zero and may cause spurious pressure oscillations after shocks are shown in Ref. 12. This spurious pressure distribution can be remedied by introducing the following first-order artificial viscosity H_s at the first downstream subsonic point after the shock

$$\begin{aligned}H_s&=-(\Delta X)(\mu p_1\phi_{XX})_X-(\Delta Y)(\mu p_2\phi_{YY})_Y\\&=(\mu p_1\phi_{XX})_{i-2m,j}-(\mu p_1\phi_{XX})_{i-m,j}+(\mu p_2\phi_{YY})_{i,j-2n}\\&-(\mu p_2\phi_{YY})_{i,j-n}\end{aligned} \tag{31}$$

By adding H_{QC} at supersonic points and H_s at first downstream subsonic points, $\mu p_1\phi_{XX}$ and $\mu p_2\phi_{YY}$ are also conserved across the shocks.

Both the nonconservative and quasiconservative schemes avoid the explicit introduction of density. For values of v of practical interest, determination of density from the velocity field is computationally costly because it requires raising a number to a fractional power. The quasiconservative approach, despite its differencing of the potential equation in a nonconservative form, has been generally found to produce results which are virtually indistinguishable from those of fully conservative schemes.[13,14]

Grid Generation

Solving the finite-difference approximation of Eq. (10) requires knowledge of mesh-point locations in the physical plane. Since only local coordinate information is used to transform the flow equation, the grid-generation step is completely uncoupled from the flow equation solver. In the present analysis, body-conforming grids are used to facilitate the treatment of body boundary conditions.

A convenient mapping function that transforms the geometry of an airfoil mounted in a channel in the physical plane (x,y) to an infinite strip of slowly varying width in the computational plane (ξ,η) is given by[8,15]

$$x+iy=\ell n[1-\cosh(\xi+i\eta)] \tag{32}$$

if the airfoil leading edge is located just upstream of the point (ℓn 2, 0). The airfoil contour is mapped to a curve near $\eta=\pi$ and the channel boundaries are mapped to near $\eta=0$. By adjusting the channel-height-to-chord ratio and choosing a small positive value of η as the channel boundary, a computational domain that extends five or six chord lengths in all directions from the airfoil can be defined. Constant ξ and η coordinate lines are chosen so that the grid points are clustered near the leading and trailing edges and near the airfoil surface. A typical grid containing 88×16 mesh cells is shown in Fig. 3 for the Korn airfoil.[16]

Boundary Conditions

There are two types of boundary conditions that must be considered in the present problem: those in the far field and those at the airfoil surface. As described in the previous section, the computational domain is truncated a finite distance from the airfoil surface. At these far-field boundaries, the solution is only slightly perturbed from the freestream conditions. A reduced potential G, representing perturbations from the freestream, is introduced according to

$$\phi=U_\infty\{x\cos\alpha+y\sin\alpha+G\} \tag{33}$$

where U_∞ is the freestream velocity and α the angle of attack. On the far-field boundaries, the values of the reduced potential are set to represent a compressible vortex of strength Γ

$$G=(\Gamma/2\pi)\arctan(y\sqrt{1-M_\infty^2}/x) \tag{34}$$

consistent with a uniformly valid asymptotic representation of the far field.[17] The value of Γ is determined iteratively by repeated application of the Kutta condition during the solution process.

At the airfoil surface, the impermeability condition

$$vx_X-uy_X=0 \tag{35}$$

is applied.

In the computational plane, Eq. (35) can be rewritten as

$$\begin{aligned}&(x_X^2+y_X^2)G_Y-(x_Xx_Y+y_Xy_Y)G_X-(x_Xy_Y-y_Xx_Y)\\&\times(y_X\cos\alpha-x_X\sin\alpha)=0\end{aligned} \tag{36}$$

The value of G at body boundary points is determined by satisfying the finite-difference approximation of Eq. (36) obtained by applying Eqs. (1), (2), and (6) at $X=0$ and $Y=1$.

For flowfields with sizable supersonic regions, the treatment of the body boundary condition near the shock needs careful consideration to insure that the solution will conserve mass flux across the shock. A simple one-dimensional analysis[13] can be performed by solving

$$(\phi_X^2-1)\phi_{XX}=0 \tag{37}$$

If $\phi_X^2\geq1$, the flow is assumed to be supersonic and an artificial viscosity is added in conservation form. A shock is found when the square of the velocity, ϕ_X^2, decreases from >1 to <1. For weak shocks, conservation of $(\phi_X^3/3-\phi_X)$ is equivalent to conservation of mass. For given boundary conditions, first- and second-order quasiconservative

solutions are obtained numerically by using second- and third-order finite-differencing schemes. The analysis shows that the second-order schemes do conserve mass flux across the shock, while the third-order schemes do not. However, if the second-order scheme is applied at the shock point and two downstream subsonic points and the third-order scheme is applied elsewhere, mass flux conservation can be preserved. The analysis also shows that the first derivative ϕ_X plays a crucial role in conserving mass flux. In the two-dimensional airfoil flow calculations, the same strategy used in the previous one-dimensional analysis is used to enforce the body boundary condition at the point of intersection of the shock with the body surface. This strategy is successful in eliminating the otherwise occurring spurious undershoots and overshoots of the static pressure distribution downstream of the shock. No special treatment is applied at nonboundary points near the shock in the third-order element scheme.

At the trailing edge, the linearized equation

$$(x_Y^2+y_Y^2)\phi_{XX}+(x_X^2+y_X^2)\phi_{YY}-2(x_Xx_Y+y_Xy_Y)\phi_{XY}=0 \tag{38}$$

is assumed to hold. Equation (38) is obtained from Eq. (10) by neglecting the nonlinear velocity contribution and the C_4 and C_5 terms. This linearized equation is strictly valid at the trailing edge only for airfoils having finite trailing-edge angles; it can be regarded as an interpolation operator when the airfoil is cusped and the second derivatives of ϕ become unbounded. The circulation Γ is determined iteratively as the solution process proceeds. A constant discontinuity in potential is applied along a branch cut (coordinate line) extending downstream from the airfoil trailing edge to the far-field boundary. The value of the discontinuity is taken as that computed at the trailing edge, thus assuring that the Kutta condition is satisfied.

Relaxation Strategies

A line relaxation scheme is developed to solve the third-order finite-difference approximation of Eq. (10) with boundary conditions specified by Eqs. (31) and (34). In the third-order finite-differencing schemes, the global truncation error of the algorithm is third-order and the approximations to the velocity components and the body boundary condition, which are expressed in terms of first derivatives of the potential function and position vectors of local mesh points, are one order more accurate than those corresponding to the conventional second-order schemes. However, the approximations of second derivatives in both the third-order and conventional second-order schemes are the same; therefore, the stability criterion, which depends mainly on the behavior of second derivative terms, is not much different in the two schemes. Care is needed, however, in the treatment of the asymmetric cross-derivative of the potential function ϕ_{XY} which tends to be destabilizing. The following method of mixing new and old values of ϕ is found to be effective in leading to a convergent process.

$$\begin{aligned}\phi_{XY}=(1/36)\{&6(\phi_{i+1,j}+\phi^+_{i,j+1})-12(\phi_{i+1,j-1}+\phi^+_{i-1,j+1})\\&+2(\phi_{i+1,j-2}+\phi^+_{i-2,j+1})-18(\phi^+_{i,j-1}+\phi^+_{i-1,j})\\&+3(\phi^+_{i,j-2}+\phi^+_{i-2,j})-6(\phi^+_{i-1,j-2}+\phi^+_{i-2,j-1})\\&+\phi^+_{i-2,j-2}+36\phi^+_{i-1,j-1}+9\phi^+_{i,j}+4\phi_{i+1,j+1}\}\end{aligned} \tag{39}$$

where ϕ and ϕ^+ are the old and new values of the potential function. The above equation holds when the line relaxation sweeps along $i=$const and in the direction of increasing i. Similar formulas can be developed for other sweeping strategies.

For the second-order nonconservative and quasiconservative schemes, second-order artificial viscosities are added at supersonic points. The old and new values of ϕ contributing to the terms $[1-(a^2/q^2)]\phi_{ss}+H_{NC}$ (or H_{QC}) of the relaxation equation are chosen to ensure a convergent process as follows:

$$\begin{aligned}[1-(a^2/q^2)]\phi_{ss}=H_{NC}=&6(\mu\rho_1)_{i,j}(C_{i,j}-C_{i-m,j})\\&+6(\mu\rho_2)_{i,j}(C_{i,j}-C_{i,j-n})+(\mu\rho_2)_{i,j}(C_{i,j}-C_{i,j+n})\\&-4(\mu\rho_1)_{i,j}(C_{i,j}-C_{i-2m,j})-4(\mu\rho_2)_{i,j}(C_{i,j}-C_{i,j-2n})+R_{ss}\end{aligned} \tag{40}$$

or

$$\begin{aligned}[1-(a^2/q^2)]\phi_{ss}+H_{QC}=&[(\mu\rho_1)_{i,j}+4(\mu\rho_1)_{i-m,j}\\&+(\mu\rho_1)_{i-2m,j}](C_{i,j}-C_{i-m,j})+[(\mu\rho_2)_{i,j}+4(\mu\rho_2)_{i,j-n}\\&+(\mu\rho_2)_{i,j-2n}](C_{i,j}-C_{i,j-n})+(\mu\rho_2)_{i,j}(C_{i,j}-C_{i,j+n})+R_{ss}\end{aligned} \tag{41}$$

where $C_{i,j}=\phi^+_{i,j}-\phi_{i,j}$ is the correction to the potential function and R_{ss} is the residual of the finite-difference approximation to $[1-(a^2/q^2)]\phi_{ss}$ evaluated using old values of ϕ.

It is also necessary in some cases to add a damping term ϕ_{st} to stabilize the equivalent time-dependent relaxation equation suggested by Jameson.[18] In the present analysis, the following term is added[3]:

$$\begin{aligned}(\beta/D^2)(V+V)\phi_{st}=(\beta/D^2)(U+V)\{&U(\phi^+_{i,j}-\phi^+_{i-m,j})\\&+V(\phi^+_{i,j}-\phi^+_{i,j-n})\}\end{aligned} \tag{42}$$

where β values from 0 to 1 are chosen depending on the strength of shock waves and mesh sizes. In subsonic flow regions, over-relaxation factors are used as in the conventional relaxation schemes.

The line-relaxation scheme is applied along either $i=$const lines or $j=$const lines. The arrangement of the third-order elements and the sweep directions are sketched in Fig. 4. In the $i=$const vertical-line sweep, the sweep starts from the leading edge and proceeds toward the trailing edge of the airfoil along both the upper and lower surfaces, and then from the trailing edge toward the far field in the downstream direction. In the $j=$const horizontal-line sweep, the sweep starts from the far field and proceeds toward the airfoil surface. To improve the convergence rate of the relaxation process, an extrapolated relaxation scheme is incorporated into the program. Two or three meshes are used; solutions obtained on coarser meshes are used as initial estimates of solutions on the next finer meshes.

Numerical Results and Discussion

Generally there are two types of errors associated with the present finite-difference solutions: the error in approximating the transformation matrix and the error in discretizing the unknown function to be solved. The error in approximating the transformation matrix depends upon the uniformity of the grid-point distribution or the distortion of local meshes in the physical plane, while the discretization error of the unknown function depends on the behavior of local gradients of the function. For the third-order isoparametric element both errors are third order.

Many reliable solutions obtained by well-established methods pertaining to transonic flowfield calculations about airfoils can be found in the literature. Therefore the present solution for airfoil flows can best be evaluated by comparing them with solutions obtained by existing methods. Perhaps

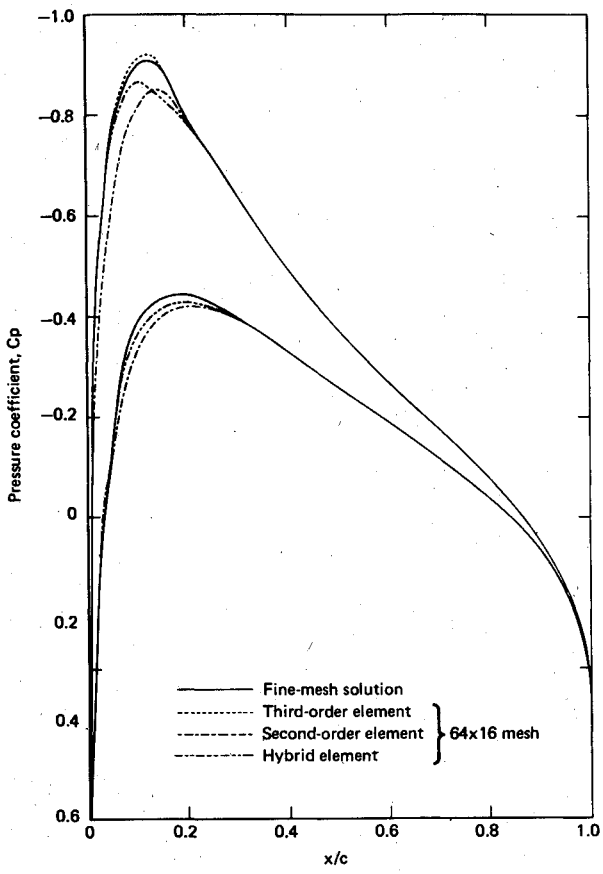

Fig. 5 Comparison of coarse- and fine-mesh solutions for a NACA-0012 at $M_\infty = 0.70$ and $\alpha = 1$ deg.

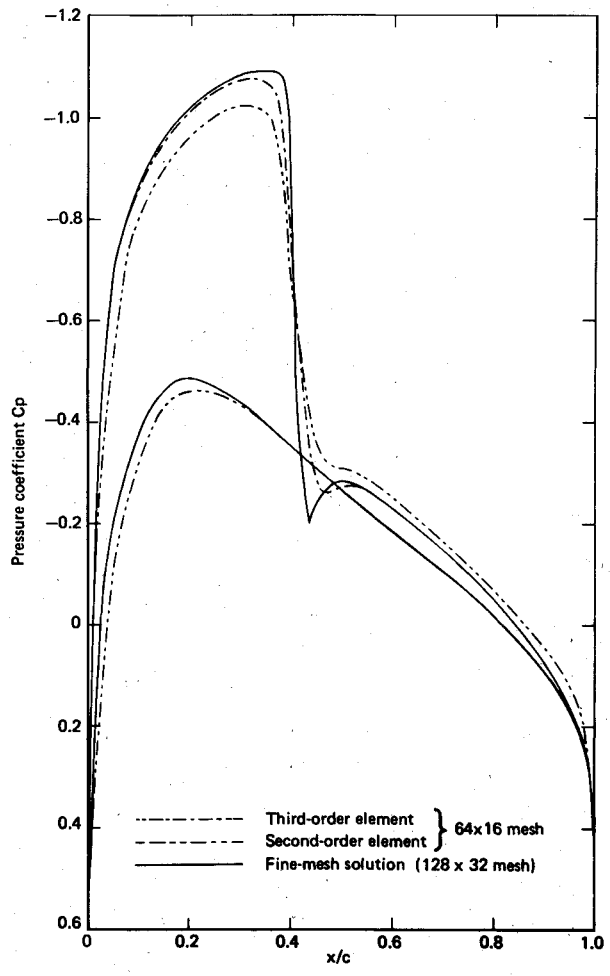

Fig. 6 Comparison of coarse- and fine-mesh solutions for a NACA-0012 at $M_\infty = 0.75$ $\alpha = 1$ deg.

the most efficient airfoil code in the public domain is FLO-36, a multigrid code developed by Jameson[19] for transonic airfoil flow calculations. In FLO-36, the O-mesh is used, and either a first- or second-order artificial viscosity (or an added term combining fractions of the first- and second-order artificial viscosities) can be used in supersonic regions to form a first- or second-order-accurate scheme. A conformal mapping procedure is applied to transform the physical domain to a polar computational domain. Since the transformation is analytical, the error of the transformation matrix is negligibly small everywhere. Comparisons of the solutions obtained by FLO-36 and the present method are made in the latter portion of this section.

A comparison of coarse- and fine-mesh solutions for a nearly subsonic flow solution is presented in Fig. 5 for the NACA 0012 airfoil at freestream Mach number $M_\infty = 0.700$ and angle of attack $\alpha = 1$ deg. Three sets of coarse-mesh solutions are obtained by the present method using 64 mesh elements around the airfoil surface, 16 mesh cells from the airfoil surface to the far field, and 12 mesh cells from the trailing edge to the downstream far field. The second- and third-order-element solutions are obtained by applying the second- and third-order elements, respectively, in both solving the flow equation and enforcing the body boundary condition; the hybrid-element solution is obtained by applying the second-order element for solving the flow equation, and the third-order element is applied to enforce the body boundary condition. In Fig. 5 the upper and lower sets of curves represent the pressure distributions on the upper and lower surfaces of the airfoil, respectively, and the coarse-mesh solutions are compared with a fine-mesh solution obtained by applying the third-order element and doubling the numbers of mesh cells in both i and j directions. The second-order-element solution underpredicts the peak C_p values on both the upper and lower surfaces, and the third-order-element solution overpredicts the peak C_p value on the upper surface by a smaller percentage error, while maintaining good agreement with the fine-mesh solution elsewhere. The hybrid-element solution is slightly better than the second-order-element solution because of the improved boundary condition; however, it still underpredicts the peak C_p values on both surfaces. In conclusion, the overall agreement is best between the third-order-element and fine-mesh solutions.

A comparison of coarse- and fine-mesh solutions for a transonic flow is presented in Fig. 6 for the same airfoil at a higher freestream Mach number, $M_\infty = 0.75$, and the same angle of attack, $\alpha = 1$ deg. Two sets of coarse-mesh solutions, obtained by the present method using the same numbers of grid points used in the previous example, are compared with a fine-mesh solution obtained by using a 128×64 mesh. All solutions are second-order quasiconservative. The third-order-element solution agrees with the fine-mesh solution almost everywhere except near the shock where the pressure jump is smeared over a wider chordwise distance because of the coarseness of the mesh. The second-order-element solution underpredicts the peak C_p values on both the upper and lower surfaces, again illustrating the improvement of solution accuracies obtained on coarse meshes using the third-order element.

All subsequent solutions obtained by the present method used 128 mesh cells along the airfoil surface, 24 mesh cells along the wake, and 32 mesh cells from the airfoil surface to the far field. Solutions are obtained after the maximum residual has been reduced by at least five orders of magnitude and the circulation change between two sweeps has been reduced to less than 0.0002%. Figure 7 shows the present solutions obtained using the second- and third-order elements

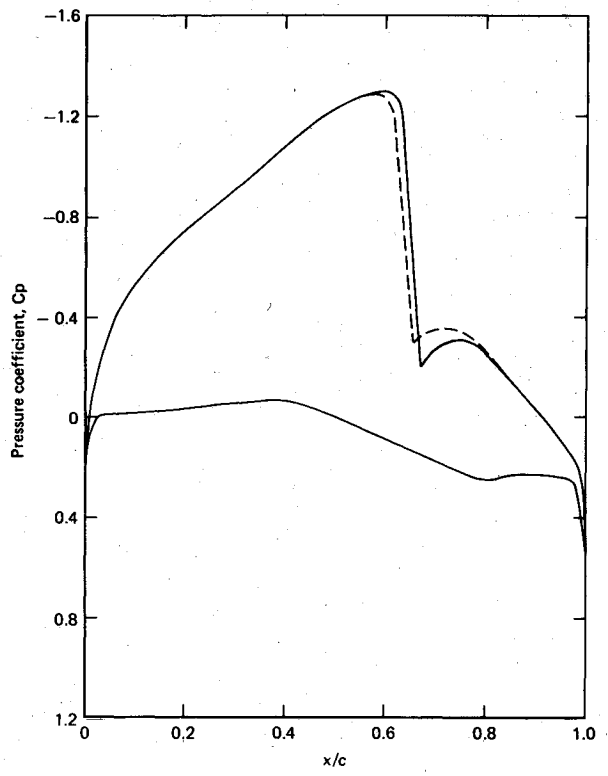

	N	M	c_L	H	Method
– – –	192	32	0.6664	First-order	Fully conservative (FLO-36)
———	128	32	0.6804	Second-order	Quasi-conservative (present)

Fig. 7 Comparison of first- and second-order solutions for a NACA 64A410 airfoil at $M_\infty = 0.74$ and $\alpha = 0$ deg.

for the NACA 64A410 airfoil at a freestream Mach number, $M_\infty = 0.75$, and angle of attack, $\alpha = 0$ deg, and compared with Jameson's fully conservative solution. In Fig. 7, N and M represent the numbers of mesh cells along the airfoil surface, and from the airfoil surface to the far-field boundary, respectively; μ represents the order of artificial viscosity added at supersonic points, and C_L is the total lift coefficient obtained from the circulation at the trailing edge. The present first-order quasiconservative solution obtained using the second-order element is in good agreement with Jameson's first-order fully conservative solution shown in Fig. 7. Nevertheless, the second-order quasiconservative solutions obtained by applying second- and third-order elements, which agree fairly well, predict stronger shock strength, slightly more downstream shock location, and a greater flow expansion after the shock. The shock strength predicted by the present second-order scheme is almost identical to the strength predicted by the one-dimensional normal shock relation. This example shows that the discrepancy existed in the prediction of shock strength and location obtained by applying the first- and second-order, quasiconservative or fully conservative schemes. The second-order quasiconservative solutions shown in Ref. 12 for the NACA 0012 and 64A410 airfoils were obtained without the proper treatment at shocks as described in Eq. (31) and predict stronger shock strengths which apparently are due to the zeroth-order errors mentioned previously.

Some airfoils are designed to be shock free at a specified freestream Mach number and angle of attack. At slightly off-

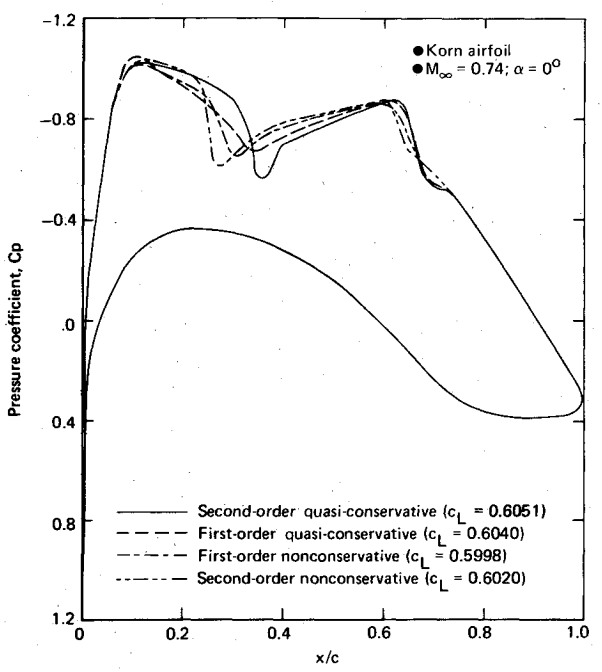

Fig. 8 Comparison of first- and second-order, nonconservative, and quasiconservative solutions using a second-order element.

design conditions, these airfoils tend to exhibit dramatic variations in static pressure distribution with small changes in Mach number or angle of attack. Therefore it is important and challenging for the finite-difference solutions to be able to capture subtle changes in the locally supersonic flows around shock-free airfoils. Figures 8-11 show solutions obtained by the present method and by FLO-36 for a Korn airfoil at $M_\infty = 0.74$ and $\alpha = 0$ deg. For this particular case, distinct double shocks appear in the second-order fully conservative and quasiconservative solutions, while the first shock near $x/c = 0.35$ tends to be smeared in the first-order solutions, even if a large number of grid points is used. Figure 8 presents comparisons of first- and second-order nonconservative and quasiconservative solutions obtained by the present method using a second-order element. The first shock is smeared over at least 10% chord length in the first-order quasiconservative solution and over about 5% chord length in the first-order nonconservative solution. The nonconservative solutions have more forward shock locations than the quasiconservative solutions; the first shock location predicted in the second-order nonconservative solution is about 8% chord upstream of the location predicted in the second-order quasiconservative solution.

Figure 9 compares the first-order fully conservative solution obtained by FLO-36 with present first- and second-order quasiconservative solutions. The second-order quasiconservative solution is obtained using a third-order element. Even with 256 mesh cells on the airfoil surface, the first shock of the first-order fully conservative solution is completely smeared.

In Fig. 10, second-order fully conservative solutions are obtained by FLO-36 using 128×32, 192×32, and 256×48 mesh cells to study the effect of mesh size upon smearing of the first shock. The first shock is completely smeared over nearly 20% chord in the 128×32 solution and becomes successively better defined in the 192×32 and 256×48 solutions. The location of the first shock predicted in the 192×32 solution is about 3% chord downstream of the location predicted in the 256×48 solution, and the strength of the first shock is also underpredicted in the 192×32 solutions. This example shows that the conventional, fully conservative schemes require a large number of grid points on the airfoil surface to adequately predict solutions with double shocks,

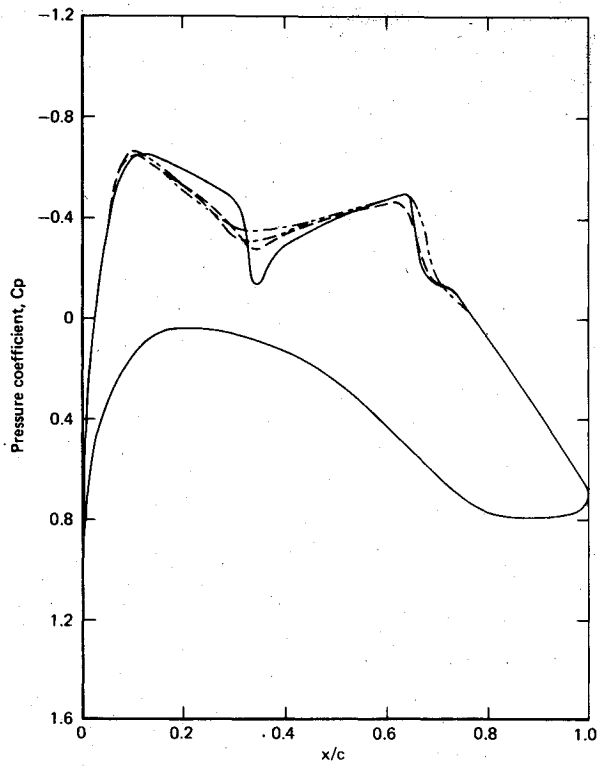

	N	M	c_L	H	Method
- - - - - -	256	48	0.5955	First-order	Fully conservative (FLO-36)
- - - - -	192	32	0.5980	First-order	
- - - -	128	32	0.6040	First-order	Quasi-conservative (MDRL
———	128	32	0.6039	Second-order	

Fig. 9 Comparison of first- and second-order solutions for a Korn airfoil at $M_\infty = 0.74$ and $\alpha = 0$ deg.

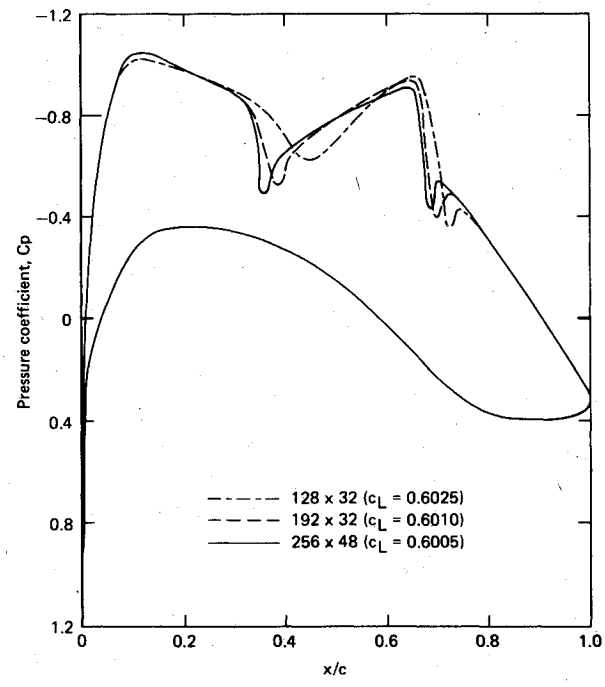

Fig. 10 Convergence study for fully conservative solutions obtained by FLO-36 for a Korn airfoil at $M_\infty = 0.74$ and $\alpha = 0$ deg.

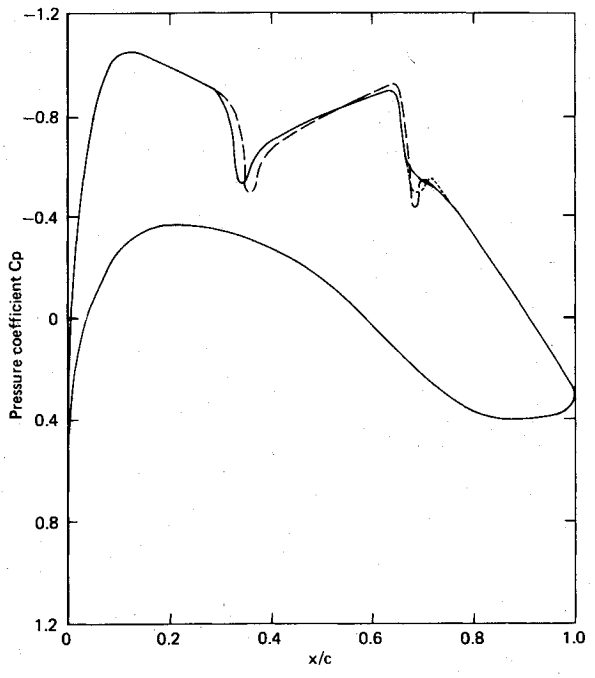

	N	M	c_L	Method
———	256	48	0.6005	Fully conservative (FLO-36)
———	128	32	0.6039	Quasi-conservative (present)
--------	128	32	0.6037	Quasi-conservative (Ref. 12)

Fig. 11 Comparison of fully- and quasiconservative solutions for a Korn airfoil at $M_\infty = 0.74$ and $\alpha = 0$ deg.

even when a second-order scheme is used. The second-order quasiconservative solutions obtained in Ref. 12 and by the present method, using the third-order element and 128 mesh cells on the airfoil surface, are presented in Fig. 11 and compared with the second-order fully conservative solution obtained by FLO-36 using 256×48 mesh cells. The agreement between the three solutions is generally good except for the discrepancies near the first and second shocks. The second-order quasiconservative solution, obtained in Ref. 12 by applying the second-order artificial viscosity H_{QC} in Eq. (30) at supersonic points and the first and second downstream subsonic points after shocks, shows a spurious pressure wiggle after the second shock. The second-order fully conservative solution also shows the same pressure wiggle. As mentioned before, this spurious pressure distribution is probably due to the zeroth-order artificial viscosity or density added at shock points. By adding the first-order artificial viscosity given in Eq. (31) at shock points, the pressure wiggle disappears in the present solution. The quasiconservative solution predicts slightly more upstream locations of both shocks, a slightly weaker strength of the first shock, and a slightly lower peak C_p of the second shock than the fully conservative solution. Because of the core memory limitation of the CYBER 175 used for the computations, the finest mesh that can be used with the FLO-36 code is 256×48; however, there is a good reason to believe that if the number of grid points used in running FLO-36 is increased beyond 256×48, the shock locations of the fully conservative solutions probably will move slightly further upstream and the peak pressure of the second shock probably will be further reduced as indicated by the trend in Fig. 10. Therefore it is believed that the present

second-order quasiconservative solution is probably closer to the exact fully conservative solution than the FLO-36 solution. Second-order quasiconservative solutions obtained using the second- and third-order elements are in good agreement except for slight differences in the shock strength. In conclusion, this study of a Korn airfoil flow demonstrates that the present second-order quasiconservative scheme is superior to the second-order fully conservative scheme in avoiding the numerical shock smearing which occurs because of poor computational resolution even with rather fine meshes.

Conclusions

A third-order isoparametric element has been successfully applied to airfoil flowfield calculations. Improved accuracy of solutions is obtained on coarse meshes, especially near the airfoil leading edge where large expansions of the flows and large curvature changes of airfoil contours occur.

The second-order quasiconservative and nonconservative schemes developed in the present study significantly improve the solution accuracy in supersonic regions. For cases containing a single shock, most solutions obtained by conventional first-order schemes nearly converge to the second-order solutions with a reasonable number of grid points. However, the present study shows that the conventional first-order schemes cannot provide accurate solutions, even with a large number of grid points, for double shock cases which are frequently observed on shock-free airfoils and highly swept wings. The second-order fully conservative scheme developed by Jameson can capture a double shock on a Korn airfoil better than his first-order scheme, but a large number of grid points is needed on the airfoil surface to adequately predict the locations and strengths of double shocks. The present second-order quasiconservative scheme has been shown to produce less numerical shock smearing than Jameson's second-order fully conservative scheme, and thus requires only half as many grid points on the airfoil surface to adequately capture double shocks.

Acknowledgments

The author would like to acknowledge Prof. D. A. Caughey of Cornell University for his fruitful discussions and comments during the course of this study and for supplying the FLO-36 code, and to F. W. Spaid for his continuous encouragement and interest in this research. This work was supported by the McDonnell Douglas Independent Research and Development Program.

References

[1] Ballhaus, W. F. and Bailey, F. R., "Computational Aerodynamics on Large Computers," *Computers and Fluids*, Vol. 8, March 1980, pp. 133-144.

[2] Lynch, F. T., "Recent Applications of Advanced Computational Methods in the Aerodynamic Design of Transport Aircraft Configurations," Douglas Paper 6639, presented at 11th Congress of ICAS, Sept. 1978.

[3] Chen, L. T. and Caughey, D. A., "A Higher-Order Finite-Difference Scheme for Three-Dimensional Transonic Flowfields About Axisymmetric Bodies," *Journal of Aircraft*, Vol. 17, Sept. 1980, pp. 668-676.

[4] Leonard, B. P., "A Survey of Finite Differences of Opinion on Numerical Muddling of the Incomprehensible Defective Confusion Equation," *Symposium on Finite Element Methods for Convection Dominated Flows*, ASME Winter Annual Meeting, New York, Dec. 1979, pp. 1-17.

[5] Jameson, A., "Transonic Potential Flow Calculations Using Conservation Form," *Proceedings of the AIAA Second Computational Fluid Dynamics Conference*, June 1975, pp. 148-161.

[6] Ives, D. C. and Liutermoza, J. F., "Second-Order-Accurate Calculation of Transonic Flow over Turbomachinery Cascades," *AIAA Journal*, Vol. 17, Aug. 1979, pp. 870-876.

[7] Chen, L. T. and Caughey, D. A., "Calculation of Transonic Inlet Flowfields using Generalized Coordinates," *Journal of Aircraft*, Vol. 17, March 1980, pp. 167-174.

[8] Jameson, A. and Caughey, D. A., "A Finite Volume Method for Transonic Potential Flow Calculations," *Proceedings of AIAA Third Computational Fluid Dynamics Conference*, June 1977, pp. 35-54.

[9] Caughey, D. A. and Jameson, A., "Numerical Calculation of Transonic Potential Flow about Wing-Body Combinations," *AIAA Journal*, Vol. 17, Feb. 1979, pp. 175-181.

[10] Chen, H. C., "Improved Surface Velocity Method for Transonic Finite-Volume Solutions," *Proceedings of the 7th International Conference on Numerical Methods in Fluid Dynamics*, June 1980; *Lecture Notes in Physics*, Vol. 141, Springer-Verlag, New York, 1981, pp. 113-118.

[11] Deconinck, H. and Hirsch, C., "Transonic Flow Calculations with Higher-Order Finite Elements," *Proceedings of the 7th International Conference on Numerical Methods in Fluid Dynamics*, June 1980; *Lecture Notes in Physics*, Vol. 141, Springer-Verlag, New York, 1981, pp. 138-143.

[12] Chen, L. T., "Higher-Accuracy Finite-Difference Schemes for Transonic Airfoil Flowfield Calculations," AIAA Paper 81-381, Jan. 1981.

[13] Caughey, D. A. and Jameson, A., "Progress in Finite Volume Calculations for Wing-Fuselage Combinations," *AIAA Journal*, Vol. 18, Nov. 1980, pp. 1281-1288.

[14] Bauer, D., Garabedian, P. R., Korn, D. G., and Jameson, A., *Supercritical Wing Sections II*, Springer-Verlag, New York, 1975.

[15] Caughey, D. A., "A Systematic Procedure for Generating Useful Conformal Mappings," *International Journal of Numerical Methods in Engineering*, Vol. 12, 1978, pp. 1651-1657.

[16] Bauer, F., Garabedian, P. R., and Korn, D. G., *Supercritical Wing Sections*, Springer-Verlag, New York, 1972.

[17] Ludford, G.S.S., "The Behavior at Infinity of the Potential Function of a Two-Dimensional Subsonic Compressible Flow," *Journal of Mathematics and Physics*, Vol. 30, 1951, pp. 117-130.

[18] Jameson, A., "Iterative Solution of Transonic Flows Over Airfoils and Wings, Including Flows at Mach 1," *Communications on Pure and Applied Mathematics*, Vol. 27, May 1974, pp. 283-309.

[19] Jameson, A., "Acceleration of Transonic Potential Flow Calculations on Arbitrary Meshes by the Multiple Grid Method," *Proceedings of AIAA 4th Computational Fluid Dynamics Conference*, July 1979, pp. 122-146.